A Method to Localize the Axial Position of Partial Discharges in GIL by Gas Sensors

Rui Qiu, Wenjun Zhou, Pascal Brault, Yu Zheng, Gen Li, Han Yang, Han Li

A Method to Localize the Axial Position of Partial Discharges in GIL by Gas Sensors

Rui Qiu, Wenjun Zhou, *Member, IEEE*, Pascal Brault, Yu Zheng, *Member, IEEE*, Gen Li, Han Yang, Han Li

***Abstract*—. This paper proposes a novel method to realize the partial discharge (PD) localizing function of gas sensors in GIL. Firstly, the diffusion characteristics of decomposition products were studied. The Fuller-Schettler-Giddings model was corrected to obtain decomposition products' diffusion coefficients in high-pressure SF_6. The finite element method (FEM) calculated the temperature rise, convection, and diffusion of decomposition products in GIL. With the relationship between the concentration variation and positions, a PD defects location method was proposed. The results indicate that the decomposition products would diffuse rapidly in the radial direction with the convection. Gas diffusion at the top of the GIL was faster than that at the bottom. Hence, the gas sensors were suggested to be set at the top of GIL. The axial diffusion was much slower and mainly affected by the temperature and diffusion coefficient. For a long GIL unit, the diffusion of decomposition products could be simplified to one-dimensional. In diffusion, the delay of the product concentration is negatively correlated with the square of the distance. That quantitative relationship could be used for localizing PD by the concentration increase delay detected by the sensors on both sides of the defect. The localization error would decrease with the increase of diffusion coefficient (rate) and prolonged monitoring (diffusion) time. The accuracy of the localization would also increase when the defect is close to the midpoint of the sensors.**

***Index Terms*—Gas-insulated transmission lines, partial discharge localization, gas diffusion, temperature rise, convection, gas decomposition, gas sensors**

I. Introduction

GAS-insulated transmission lines (GIL) have advantages such as high voltage levels and good mechanical flexibility [1], [2], [3]. However, partial discharge (PD) is the main problem affecting the stability of GIL [4], [5]. The long axial distance of GIL also makes defect localization essential and challenging. As one of the gas analysis technologies, the gas sensors could distinguish the PD defect by monitoring the variation of gas components [6], [7]. However, same with other gas analysis methods (e.g., gas chromatography [8], infrared absorption spectroscopy [9]), gas sensors still have a shortcoming in localizing PD. That also severely limits the use of gas sensors on the GIL. It is necessary to use other technologies (e.g., traveling wave [10], optics [5], ultra-high-frequency methods [11], and ultrasonic methods [12]) to localize the PD. However, some weak PDs are challenging to be monitored by above-mentioned localization methods but could be detected by gas analysis techniques. Therefore, if the PD localization function of gas sensors could be realized, the application and role of gas sensors in GIL insulation diagnosis could be improved.

According to the detection principle, gas sensors could be divided into photoacoustic spectroscopy sensors [13], [14], nanotube sensors [7], [15], etc. Gas sensors were first applied to gas-insulated switchgear (GIS). Due to the compact structure of the GIS chamber, the defect location function of the gas sensor received little attention. However, in the long distance and large volume of GIL chamber, the gas components in different positions vary significantly. The position of the gas sensor arrangement becomes important. The gas sensors could also realize the PD localization by the difference in gas components difference in different positions. That requires the clarification of gas diffusion procession in GIL [16]. Due to the difficulty in obtaining diffusion coefficients, the current research on the diffusion process of decomposition products in GIL was limited [17], [18]. Ming et al. predicted the diffusion coefficients of eight decomposition products by molecular volume and the Fuller-Schettler-Giddings (FSG) model [19]. The FSG model has significant errors under high pressure. Therefore, the accuracy of the prediction results needs to be verified. Our team also tested the diffusion process of decomposition gases in GIL [16]. The diffusion coefficients of SO_2F_2 and SO_2 in SF_6 were measured. However, there are diverse decomposition products in SF_6. Enriching diffusion coefficients for different decomposition products under high pressure is still necessary.

In addition, the abovementioned research ignored the temperature and convection on gas diffusion in the GIL. In operation, heat would be generated by the current in the GIL conductor. The heat transmission in the gas would generate convection. Then, the temperature and convection would affect the molecular thermal motion and gas transport processes, respectively. Therefore, in order to accurately simulate the diffusion process in GIL, it is also important to study thermal convection. The related experiment and simulation research is adequate and referable. For example, Ham et al. analyzed the temperature rise into the GIL by heat balance equation, finite elements methods (FEM), and temperature rise test, respectively. They found that the fluid dynamics simulation results were closer to the experimental results [20]. The temperature rise test of 550 kV GIL was carried out by

This work was supported in part by the National Key R&D Program of China 2021YFB2401400 and Science and Technology Project of China Southern Power Grid Co., Ltd. 090000KK52210175. (*Corresponding author: Wenjun Zhou*).

Rui Qiu, Wenjun Zhou, Yu Zheng, Gen Li, Han Yang and Han Li are with the School of Electric Engineering and Automation, Wuhan University, Wuhan 430072, China (e-mail: wjzhou@whu.edu.cn).

Rui Qiu and Pascal Brault are with the GREMI, UMR 7344 CNRS & Université d'Orléans, Orléans BP6744, France.

Minaguchi [21]. The temperature rise calculation results could be consistent with the experimental data well. Those researches provide the crucial basis for simulating the diffusion characteristics of decomposition products in GIL with temperature rises and convections. That could also provide the relationship between the variation and position of the components, the basis for localizing PD defects by gas sensors.

In this paper, we tried to determine the diffusion coefficients of some decomposition gases through experiments. Then, the existing FSG model to predict diffusion coefficients could be modified for high-pressure conditions. Furthermore, finite element simulation could analyze the temperature rise, convection, and diffusion in GIL. A novel method for localizing the PD defects in GIL would be proposed based on the diffusion characters from the above results and models.

II. Setup of Simulation and Experiment

As illustrated in Fig. 1, the diffusion process is promoted by two main factors: the concentration gradient and the flow. The diffusion coefficients determined the diffusion rate for different components driven by the same gradients. In addition to the properties of the components, the diffusion coefficient is affected by pressure and temperature. When the temperature rise happens in the gas, with the heat transfer, the convection would also be promoted. Hence, the temperature rises in gas affected the diffusion via flow and concentration gradient.

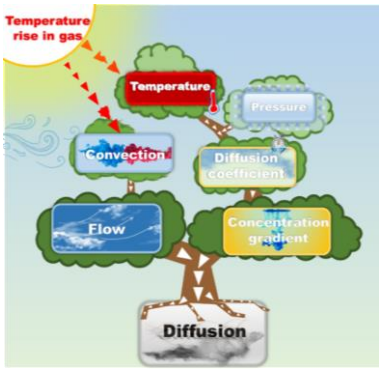

Fig. 1. The main factors of the diffusion process.

According to the Fig. 1, the diffusion process of decomposition products in GIL could be analyzed via Fick's second law [22]:

$$\frac{\partial C_{\mathrm{d}}}{\partial t}-D_{\mathrm{pd/SF6}}\left(\nabla^{2}\mathrm{C}_{\mathrm{d}}\right)+v\nabla\cdot C_{\mathrm{d}}, \tag{1}$$

where t (h) is the time, C_{d} (ppm) is the concentration of decomposition products, v is the flow velocity (m/s), and $D_{\mathrm{pd/SF6}}$ ($\mathrm{m^2/S}$) is the diffusion coefficient of decomposition products in SF_6. The basis for solving (1) lied in obtaining $D_{\mathrm{pd/SF6}}$ and v.

A. Method to obtain diffusion coefficient

The optimized Fuller-Schettler-Giddings (FSG) model was used to calculate and predict the diffusion coefficient $D_{\mathrm{d/SF6}}$ [16]:

$$D_{\mathrm{pd/SF_6}}=K_{\mathrm{pd/SF_6}}\cdot\frac{T^{1.75}}{P}=k_{\mathrm{r}}\cdot K_{\mathrm{pr/SF_6}}\cdot\frac{T^{1.75}}{P}, \tag{2}$$

where $K_{\mathrm{pd/SF6}}$ is the diffusion characteristic coefficient, $K_{\mathrm{pr/SF6}}$ is the diffusion characteristic coefficient of the reference product, k_{r} is the ratio of $K_{\mathrm{pd/SF6}}$ to $K_{\mathrm{pr/SF6}}$ in [16], [19], T (K) is the temperature, and P (Pa) is the absolute gas pressure. T was related to the temperature distribution in GIL. Pressure assumed to be a constant in this paper, is determined by the GIL voltage level. In this paper, SO_2F_2 was chosen as the reference decomposition product [8]. The diffusion experiments were introduced to determine the $K_{\mathrm{pr/SF6}}$ of SO_2F_2. In Fig. 2, the experiment platform consisted of a diffusion chamber and a GC-9760B gas chromatography. The diffusion chamber was equipped with sampling points A and B. They were spaced 1 m apart, which could detect the concentration difference leaded by diffusion. The diffusion source located at 0.5 m from point A. The chamber and diffusion source were inflated with equal pressure of SF_6 and SO_2F_2, respectively. The pressure was 0.35 MPa, 0.40 MPa, and 0.45 MPa, the diffusion time was 108 h, and the sampling period was 12 h.

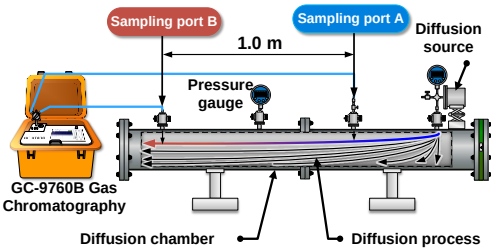

Fig. 2. Diffusion experiments platform.

B. Temperature rise, convection, and diffusion simulation model in GIL radial direction

Since the axisymmetric structure of GIL, the temperature rises and convection in GIL are mainly in the radial direction. Hence, a two-dimensional radial model was introduced [17], [18], [20]. The GIL has two heat sources: the conductor (load current heat) and the shell (induction current heat). The fluid heat transfers would induce temperature gradients and convection.

According to Maxwell's equations, the electromagnetic field in the GIL satisfies:

$$\begin{cases}\nabla^{2}\mathrm{A}_{\mathrm{n}}-j\omega\mu\chi(T)\mathrm{A}_{\mathrm{n}}=\mu\mathrm{J}_{\mathrm{s}}\ \text{(conductor)}\\ \nabla^{2}\mathrm{A}_{\mathrm{n}}=0\ \text{(shell)}\end{cases} \tag{3}$$

where $\boldsymbol{A}_{\mathrm{n}}$ (Wb/m) is the magnetic vector perpendicular to the GIS radial section, $\boldsymbol{J}_{\mathrm{s}}$ ($\mathrm{A/m^2}$) is the current density inside the conductor, ω (rad/s) is the angular frequency, μ (H/m) is the permeability, $\chi(T)$ ($\mathrm{S/m^2}$) is the material conductivity related to temperature T:

$$\chi(T)=\chi_{0}/(1+0.004(T-273)), \tag{4}$$

where χ_0 is the material's electrical conductivity at 273 K. For 6063 aluminum alloy used for GIL, χ_0 is 55 $\mathrm{S/m^2}$. The tangential component of the air edge magnetic vector is 0 Wb/m. The heat generation Q of the conductor and shell is

$$Q=\int_{S}\left(\left|\boldsymbol{J}_{\mathrm{s}}-j\omega\sigma(T)\boldsymbol{A}_{\mathrm{n}}\right|^{2}/\chi(T)\right)\mathrm{d}S, \tag{5}$$

In GIL, three types of heat transfer work: conduction, radiation, and convection. The conduction mainly occurred in the conductor and shell. The radiation appeared on the surfaces of the conductor and shell. The convection primarily exists in SF_6 and Air. The conduction process could be solved by (6).

Where λ_s ($W \cdot m^{-1} \cdot K^{-1}$) is the thermal conductivity of solid material, and Q_v (W/m) is the volumetric heat source:

$$Q_v = -\lambda_s \nabla^2 T . \tag{6}$$

The conservations of mass, momentum, and energy in controlled the heat transfer process by the convention. (7)

$$\begin{cases} \nabla \cdot \left(\rho_g \boldsymbol{v} \right) = 0 \ \text{(mass)} \\ \rho_g (\boldsymbol{v} \cdot \nabla)\boldsymbol{v} = \nabla \cdot \left(-P \cdot \boldsymbol{E} + \vartheta \left(\nabla \boldsymbol{v} + (\nabla \boldsymbol{v})^{\mathrm{T}} - 1.5\vartheta(\nabla \boldsymbol{v})\boldsymbol{E} \right) \right) + g\Delta\rho_g \ \text{(momentum)} \\ \rho_g \Gamma \boldsymbol{v} \nabla T = \lambda_g \nabla^2 T + Q_v \ \text{(energy)} \end{cases} ,$$

where $\boldsymbol{v}$ (m/s) is the gas flow vector at the conductor and shell surfaces, $\boldsymbol{v}$ = 0 m/s; Γ ($J \cdot kg^{-1} \cdot K^{-1}$) is the heat capacity of the gas material, ρ_g (kg/m^3) is the gas density, λ_g ($W \cdot m^{-1} \cdot K^{-1}$) is the gas thermal conductivity, ϑ (Pa·S) is the viscosity. λ_g and ϑ could be calculated by Sutherland's law[22]:

$$\begin{cases} \lambda_g = \lambda_0 \left(\dfrac{T}{273} \right)^{1.5} \dfrac{273 + Su}{T + Su} \\ \vartheta = \vartheta_0 \left(\dfrac{T}{273} \right)^{1.5} \dfrac{273 + Su}{T + Su} \end{cases} \tag{8}$$

where λ_0 and ϑ_0 are gas thermal conductivity and viscosity at 273 K, and *Su* is the Sutherland temperature. The radiative heat transfer between the outer surface of the conductor and the inner surface of the shell could be solved by the Stefan-Boltzmann law:

$$-\lambda_S \nabla T = \sigma \varepsilon F_{ij} \left(T_i^4 - T_j^4 \right), \tag{9}$$

where σ is the Stefan-Boltzmann coefficient, 5.67×10^{-8} $W \cdot m^{-2} \cdot K^{-4}$; T_i and T_j are the temperatures of units *i* and *j*, ε is the unit emissivity, and F_{ij} is the angular coefficient between units *i* and *j*. Furthermore, the radiative heat transfer of the shell's outer surface to the air could be:

$$-\lambda_s \nabla T = \sigma \varepsilon \left(T_i^4 - T_j^4 \right). \tag{10}$$

This paper set up a finite element model in Fig. 3 according to the abovementioned equations and a 550 kV GIL. The free triangular mesh was used with a maximum size of 255 mm. The model had a total of 20644 units. The parameters set are elaborated in Table I. Based on the temperature rise simulation results and (2), the $D_{P/SF6}$ at different radial positions could be obtained. The radial diffusion process was simulated based on the convection results and the diffusion models in (1). The fluxes on the conductor's outer surface and the shell's inner surface are 0 ppm·m/s. The concentration at the defect $C_{ds}(t)$ was assumed to increase linearly with time.

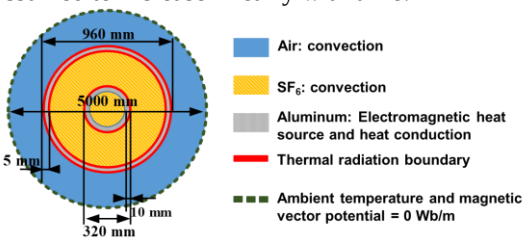

Fig. 3. GIL temperature rises model settings.

TABLE I

MATERIALS PARAMETERS IN THE MODEL

Parameters (273 K)	SF_6	Air	conductor/shell
ρ (kg/m^3)	22.82	1.293	2730
λ_0 (10^{-2} $W \cdot m^{-1} \cdot K^{-1}$)	1.206	2.44	220(λ_s)
ϑ (10^{-5} Pa·s)	1.42	1.72	/
Γ ($J/kg \cdot K$)	665.18	1005	880
ε	/	/	0.8/0.9
Su (K)	243.8	110.4	/

C. Diffusion simulation model in GIL axial direction

As mentioned, temperature and convection differences are negligible in the GIL axial direction. Hence, the radial temperature rises and convection simulation results could be the constant conditions in the 3-dimensional axial diffusion model in Fig. 4. The length of the GIL model is about 100 m [16]. The decomposition products flow in from one side and out to the other. The diffusion time is 100 h. A free tetrahedral grid dissection was used. The maximum length of the cells is 10 mm, and there are 2378487 cells in the model.

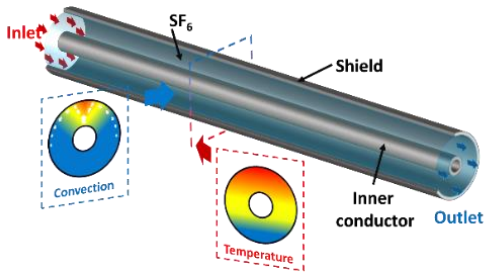

Fig. 4. GIL axial diffusion model.

The flow chart of the simulation and experiments in this paper are shown in Fig. 5.

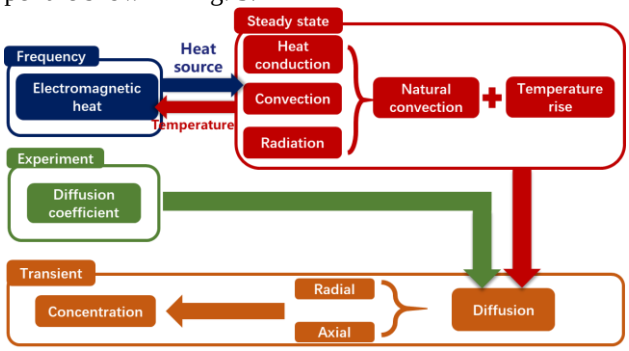

Fig. 5. Simulation and experiment flow chart.

III. RESULTS

A. Diffusion experiment results and diffusion coefficients

Fig. 5 indicates the SO_2F_2 concentration at sampling points A and B under different time and pressures. The SO_2F_2 concentration increased slowly over time. Higher pressure would slow down the diffusion. The diffusion delays Δt_{SO2F2} were 2.314 h, 2.663 h, and 3.025 h, respectively, when the pressure was 0.350 MPa, 0.400 MPa, and 0.450 MPa. With the diffusion distance of 1 m, the relationship between the diffusion coefficient and diffusion

delay is [16]:

$$D_{pd/SF6}=2.077\times10^{-4}/\Delta t. \quad (11)$$

Based on (2), (8), and Fig. 6, the $K_{pr/SF6}$ could be calculated as 1.521×10^{-3}. According to the k_r in [15], the $K_{pd/SF6}$ of 8 specific decomposition products: HF, H_2S, SO_2, SOF_2, SO_2F_2, S_2OF_{10}, CS_2, and COS were predicated and listed in Table II. In addition, the $D_{pd/SF6}$ of SO_2F_2 and SO_2 in [16] is 1.113×10^{-4} m^2/s and 1.397×10^{-4} m^2/s, respectively. The prediction value in this paper was 1.119×10^{-4} m^2/s and 1.444×10^{-4} m^2/s. Their relative differences were 0.539% and 3.255%. The prediction values of diffusion coefficients in this paper are close to the experiment one.

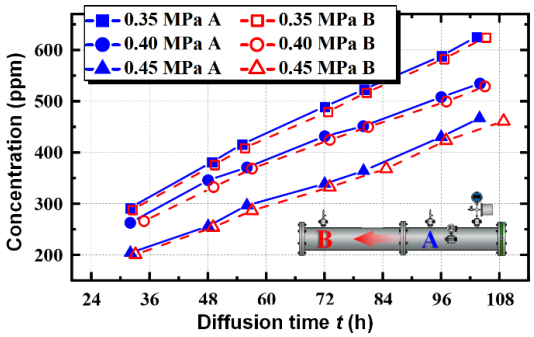

Fig. 6. The concentration variation of SO_2F_2 at sampling points A and B under different pressure.

TABLE II
DIFFUSION CHARACTERISTIC COEFFICIENTS

Products	$K_{pd/SF6}$	Products	$K_{pd/SF6}$
HF	4.82×10^{-3}	SO_2F_2	1.52×10^{-3}
H_2S	2.62×10^{-3}	S_2OF_{10}	8.98×10^{-4}
SO_2	1.96×10^{-3}	CS_2	1.60×10^{-3}
SOF_2	1.69×10^{-3}	COS	1.90×10^{-3}

B. Radial temperature rise and convection

The calculation results were compared with the experimental data at 2.6 kA, 4.4 kA, and 5.6 kA, respectively. Table III demonstrates the comparison results. Their average relative error is 2.75 %. The accuracy of the temperature rise models in GIL is receptible.

TABLE III
COMPARISON BETWEEN THE CALCULATION AND EXPERIMENT RESULTS OF 550 KV GIL TEMPERATURE RISES

Current (kA)	The temperature rises (°C)							
	Top conductor		Bottom of conductor		Top of shell		Bottom of shell	
	Exp	Cal	Exp	Cal	Exp	Cal	Exp	Cal
2.6	41	41	41	41	34	33	31	32
4.4	57	60	57	59	37	37	32	34
5.6	84	90	84	89	56	57	46	52

The simulation result of a 550 kV GIL temperature rise at 5.6 kA is visible in Fig. 7(a). The highest temperature was 86.7 °C at the conductor, and the lowest was 48.3 °C at the bottom of the enclosure. The temperature distribution in the GIL had a symmetry characteristic, and the gas temperature gradually decreased from top to bottom. Fig. 7(b) illustrates the distribution of convection. The flow velocity at the top of the conductor and shell was the largest. The flow velocity at the bottom of the chamber was low. That could be because the SF_6 near the conductor heats up fast. The decreased density caused by heating would make this part of SF_6 first overcome gravity to move upwards. When the heated SF_6 arrives at the shell, it would slide along the inner surface. In addition, a larger temperature gradient would lead to more convection. Hence, the high-speed area was mainly concentrated on the top of GIL. There was almost no convection in the low-temperature region at the bottom of GIL.

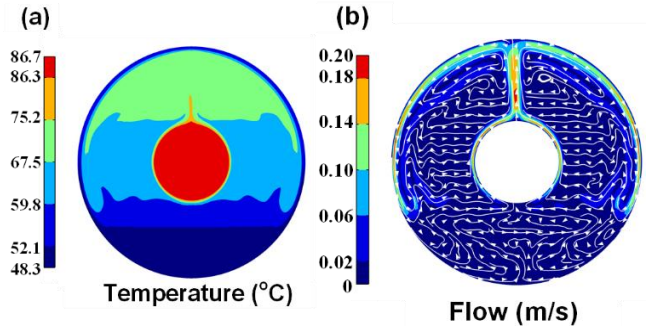

Fig. 7. The distribution of the temperature and convection in 550kV GIL at 5.6 kA. (a) The temperature distribution. (b) The convection distribution, and arrows indicate flow directions.

C. Radial diffusion characteristics of SF_6 decomposition products in GIL

Six defect positions (gas inlets): **a**, **b**, **c**, **α**, **β** and **γ**, were set on the conductor and shell individually. The generation rate of decomposition products was 0.1 ppm/h. Due to the temperature rise, the diffusion coefficients distribution of 8 decomposition productions are shown in Fig. 8. It was similar to the temperature distribution in Fig 7(a).

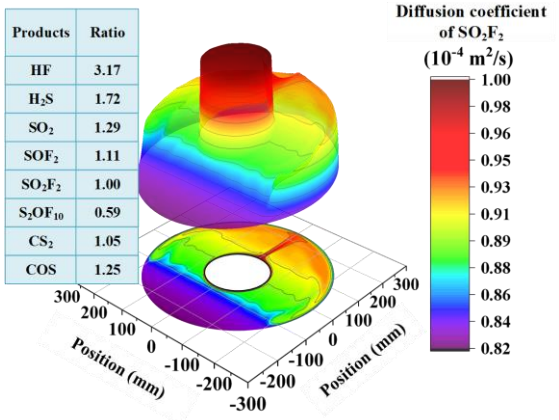

Fig. 8. The distribution of diffusion coefficients.

Fig. 9(a) and Fig. 9(b) display the diffusion range with and

without the temperature rise and convection at 0.85 h, respectively (case, the defect was at **a** point). The temperature rise and convection would manifestly promote decomposition products to diffuse uniformly. Based on the (1) and (2), it could be inferred that a higher temperature rise in GIL could lead to a faster radial diffusion. In addition, the difference in diffusion coefficients did not cause the different diffusion characteristics of decomposition products in Fig. 9(b). It suggests that convection is the primary factor in the radial diffusion, and the temperature rise is the secondary one. That could help to improve the synchronization of the radial monitoring of GIL decomposition products.

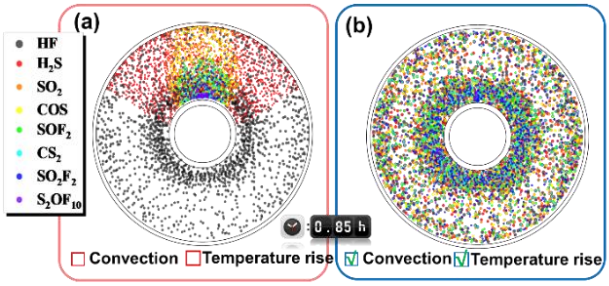

Fig. 9. The distribution of diffusion coefficients and decomposition products. (a) The diffusion range with the temperature rise and convection. (b) The diffusion range without the temperature rise and convection.

Fig. 10 illustrates the SO_2F_2 concentrations on the GIL shell when the defect was at different positions after 2h diffusion. In this paper, the difference between the concentration detected by sensors and that at defects is called the error. The relative error with defects at **a**, **b**, **α** and **β** were small, only 9.79%, 5.52%, 7.01% and 17.99%, respectively. That may be due to because the strong convection at the top of GIL. Conversely, when the defects were at the bottom **c** and **γ** points, where convection was weak and temperature was low, the relative errors increased to 34.71 % and 34.21 %. In the case of defects at **c** and **γ**, the anisotropy problem in monitoring results was also noticeable.

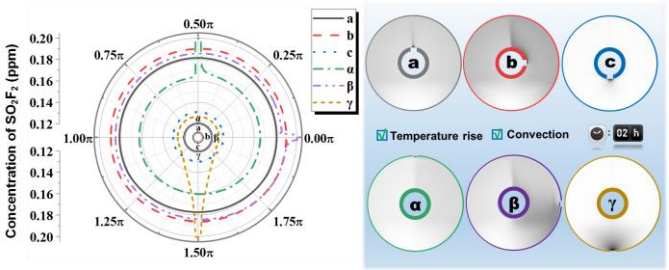

Fig. 10. The SO_2F_2 concentration on the GIL shell for different defect positions.

In summary, GIL temperature rise and convection could diffuse the decomposition products rapidly, simultaneously, and uniformly in the radial direction. Moreover, convection is the primary factor in the radial diffusion. At the top of GIL, with high temperature and strong convection, the difference results could be more accurate and faster. While the temperature rises and convection at the bottom of GIL are weak. The diffusion process is slow, resulting in a large difference between the concentration of decomposition products at the defect and that detected by the gas sensors. Therefore, it was suggested that the gas sensors are set at the top of the GIL.

D. Axial diffusion characteristics of SF_6 decomposition products in GIL

The rapid radial diffusion and the large difference in radial-axial dimensions would allow the decomposition products to have diffused in uniform in the radial direction at the beginning of the axial diffusion [16]. Therefore, this paper ignored the radial distribution of decomposition products at the beginning of axial diffusion. The cross-section at the inlet was a diffusion source (generation rate: 0.1 ppm/h). α, β, γ lines, and αe, βe, γe points were at the top, middle, and bottom of the shell. αe, βe, γe points were 5m away from the inlet. These lines and points were used to investigate concentration distribution and variation characteristics during the axial diffusion. Fig. 11(a) illustrates the concentration distribution in the first 5m on the α line after 100h of diffusion. The concentration decayed exponentially with the increase in the axial distance [16]: a smaller $D_{dp/SF6}$ would lead to more decay. Fig. 11(b) shows an apparent diffusion delay in the concentration variation at αe. The delay was also negatively correlated with $D_{dp/SF6}$.

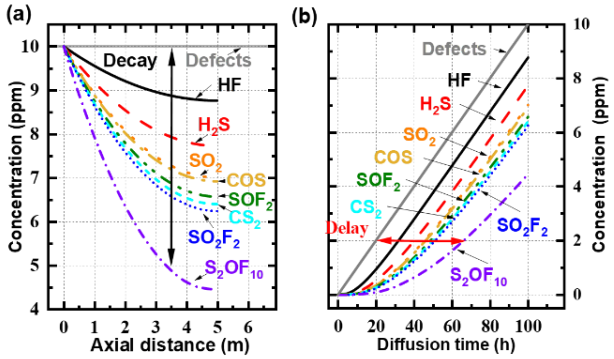

Fig. 11. The decay and delay of decomposition products concentration in axial diffusion. (a) Decay. (b) Delay.

The distributions of SO_2F_2 concentration on α, β, and γ lines are illustrated in Fig. 12. It suggested that, the effect of temperature rise and convection on axial diffusion could be neglected. That was because the convection vector had no axial component. Hence, $D_{dp/SF6}$ and temperature mainly controlled the axial diffusion. However, $D_{dp/SF6}$ was stable under high pressure. Even the temperature at the top was higher than that at the bottom, see Fig. 7(a), the $D_{dp/SF6}$ of SO_2F_2 at the top of GIL was only 9.98×10^{-5} m^2/s, which close to the bottom one of 8.25×10^{-5} m^2/s. Therefore, the concentration in the radial direction was almost the same everywhere during the axial diffusion. In addition, the average temperature rise in radial cross-section was used to calculate $D_{dp/SF6}$ and the axial diffusion model, i.e., the 3D model was simplified to 1D. Fig. 12 indicates that the difference between the 1D and 3D models was around 0.001 ppm. The axial diffusion process of the decomposition products in GIL could be approximated by a 1D

model. That also proved that the conclusions and results in [16] could be referenced.

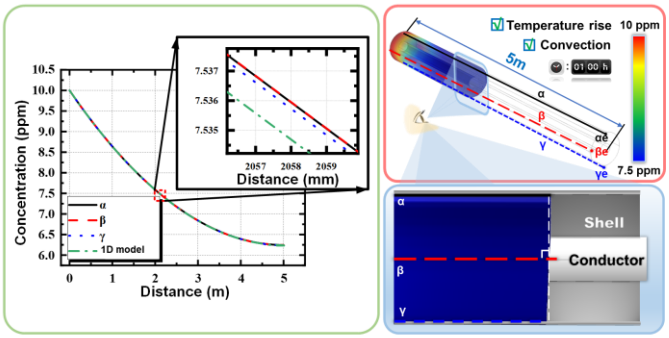

Fig. 12. The distribution of SO_2F_2 concentration on α, β, and γ lines, and the snapshot of axial diffusion process.

Based on the models in [16], in a 100 m GIL unit, the decay and delay of the concentration could be:

$$\begin{cases} C_{dM} = C_{dD} \cdot \eta = C_{dD} \cdot \exp(-0.021x/\sqrt{\pi t \cdot D_{pd/SF6}}) \\ \Delta t = (-1.389\times10^{-4}(x-100)^2 + 1.389)/D_{pd/SF6} \end{cases}, \quad (12)$$

where x (m) is the distance, C_{dD} and C_{dM} (ppm) are decomposition product concentrations at defects and gas sensors, t (h) is the time, and η is the decay ratio. The axial diffusion is mainly affected by the diffusion coefficient. The concentration decay and delay caused by axial diffusion are more significant. Therefore, axial diffusion would affect the monitoring results of gas sensors severely. However, that significant difference in concentration variation due to axial diffusion could help to do the axial localization of PD defects.

IV. The Method to Localize Axial Position of Partial Discharge in GIL by Gas Sensors

The above section gave the decay and delay characteristics of the decomposition products concentration in GIL. That could help to determine the position of PD via the difference in the concentration detected by gas sensors. As shown in Fig. 13, the gas sensors were arranged at 20 m spacing in a 100m GIL unit [16]. That scheme ensured the presence of at least one sensor on each side of the defect. The GIL unit could be flexibly divided into several 20m-long monitoring segments. The sensor on the left side of the PD was LS, and the right one was RS. When the PD distanced LS and RS were equal, i.e., the defect occurred in the midpoint of the two sensors, the concentration detected by LS and RS varied consistently. In converse, there would be a difference in the variation of the concentrations detected by LS and RS. Based on (12), the distance between the PD and LS and the distance between PD and RS satisfied:

$$\begin{cases} L_{LS} = 10 - \Delta t_{LR} D_{dp/SF6} \times 20 \\ L_{RS} = 20 - L_{LS} \end{cases}, \quad (13)$$

where Δt_{LR} (h) is the delay between monitored concentrations at LS and RS to reach the same concentration, L_{LS} (m) is the distance between the defect and LS, and L_{RS} is the distance between the defect and RS. L_{LS} + L_{RS} = 20 m (the gas sensors spacing).

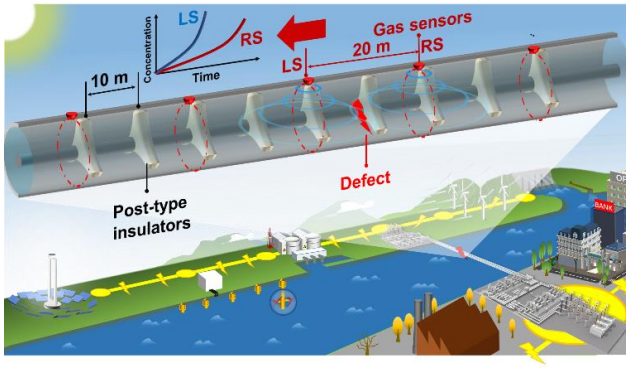

Fig. 13. An arrangement of sensors in a 100m GIL.

V. Discussions

A. Interference of overheating faults on PD localization

Localized overheating fault may occur with PD together. It could cause the diffusion coefficients to be larger than prediction. To confirm the local overheating, the diffusion coefficient could be determined by introducing data from the third sensor. In this case, the distance between the third sensor and LS or RS was 20 m. According to the simulation model in [16], the Δt of 20 m diffusion distance could be:

$$D_{dp/SF6}=0.345/\Delta t. \quad (14)$$

If the measured diffusion coefficient was larger than the predicted one, it could be inferred that GIL have localized overheating faults. When the temperature is hard to obtain for calculating diffusion coefficients, online measurement of diffusion coefficients could also be a alterative solution. However, the presence of a temperature gradient by localized overheating may cause diffusion coefficients change in the axial direction. The localization accuracy may be worse. That will be further studied in our future works.

B. Accuracy of PD localization method

To analyze the accuracy of the method, a series of simulations were done with different diffusion time, PD positions, and diffusion coefficients. The L_{LS} was set as 2.5m, 5m, 7.5m, and 10m, respectively. Considering the symmetric equivalence, this paper did not specifically list the models with L_{LS} over 10m (e.g., the case of L_{LS} = 2.5m, i.e., L_{RS}=17.5 m, is same with that of L_{LS} =17.5m). According to the Table II, $D_{dp/SF6}$ was 5×10^{-4} m^2/s, 1×10^{-3} m^2/s, and 5×10^{-3} m^2/s. The generation rate was set as 10 ppm/h. For the different $D_{dp/SF6}$, the diffusion time was adjusted from 100h to 10000h. The localization errors are illustrated in Fig. 14. It could be found that the localization error was decreasing due the prolonged diffusion time (see Fig. 14(a) and Fig. 14(d)). In Fig. 14(b), the increase of diffusion coefficients could help to reduce localization errors. That could be explained by the following. (13) was established on the premise that the increase gradient of the concentration was stable. The diffusion delay would not vary during the diffusion process. However, as shown in Fig. 9(b), it would take some time for the concentration growth rate to stable. Until the stabilization, the delay would increase with

the prolonged diffusion time. In that case, the localization result of (13) would be inaccurate due to an unstable diffusion delay. As the diffusion time increases, the delay becomes stable, and the accuracy of (13) gradually increased. A higher diffusion coefficient would accelerate diffusion delay stabilization. Hence, a longer diffusion time and a larger diffusion coefficient would make localization more accurate. That is also the main reason why a larger diffusion coefficient resulted in a shorter required time for the error limitation in Fig. 14(c). In addition, the method has more accuracy for PD defects close the PD is to the midpoint between gas sensors. That is because the closer to the midpoint, the less the difference in concentration detected by two sensors. Then, the unstable delay has less effect on (13).

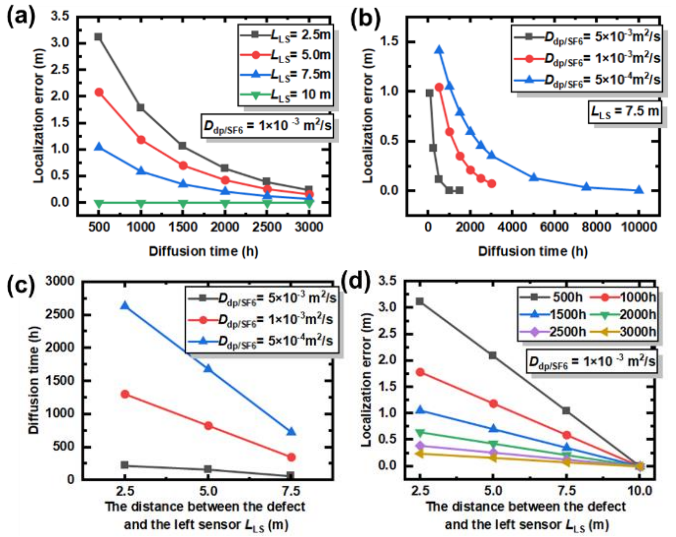

Fig. 14. The localization errors under different conditions. (a) Variations of errors with diffusion time. (b) Effects of diffusion coefficients on the variation of error. (c) The minimum diffusion time for the accuracy above 90%. (d) The errors at different PD positions.

In fact, Fig. 13 only disclose the theoretical error of the localization methods. There would be more disturbances and factors in the diffusion process in GIL (e.g., axial convection and temperature gradient). In addition, the insulators, especially the supporting one, would obstacle the diffusion process. That requires further simulation and experimental analysis. Our team would also conduct further research on the simulation with more details and the validation experiments on a real GIL in the future. Nevertheless, this paper still could demonstrate the feasibility of localizing PD defects through the gas sensors.

VI. Conclusions

The modified FSG model could predict the diffusion coefficients of decomposition products in high-pressure SF_6. Among the eight typical decomposition products in SF_6, HF had the fastest diffusion rate. The diffusion coefficients of H_2S, SO_2, COS, SOF_2, CS_2, and SO_2F_2 were similar. They could be monitored and compared for simultaneous analysis.

Under the effect of temperature rise and convection, the radial diffusion of decomposition products was fast. In contrast, axial diffusion is only affected by temperature and slow. The diffusion rate of decomposition products at the top of GIL was higher than at the bottom. The arranging gas sensors at the top of the GIL was suggested. For the slow axial diffusion, it has more concentration decay and diffusion delay, which lead to gas monitoring accuracy and timeliness problems. According to the simulation results, the diffusion process could be simplified to a 1-dimensional model. The diffusion coefficient could be determined by the average temperature rise.

Diffusion delays have a quantitative relationship with the diffusion distance in the form of a quadratic function. With that relationship and the gas sensors' axial array, the defect could be localized by the concentration delay detected by the sensors on both sides of the PD defect. Localization accuracy is positively correlated with diffusion coefficient and diffusion time. In addition, the localization accuracy would increase when the defect is close to the midpoint of the sensors. If the gas diffusion is slow, a longer monitoring time is necessary for high accuracy.

References

[1] H. Koch, F. Goll, T. Magier and K. Juhre, "Technical aspects of gas insulated transmission lines and application of new insulating gases," *IEEE Trans. Dielectr. Electr. Insul.*, vol. 25, no. 4, pp. 1448-1453, Aug. 2018, doi:10.1109/tdei.2018.007311.

[2] C. Tateyama, T. Kobayashi, A. Kumada and K. Hidaka, "Conceptual Design and Feasibility Study of Flexible Gas-Insulated Transmission Line Using CF3I Gas Mixture," *IEEE Trans. Dielectr. Electr. Insul.*, vol. 28, no. 4, pp. 1424-1430, Aug. 2021, doi: 10.1109/tdei.2021.009605.

[3] H. C. Liang, B. X. Du, and J. Li, "Electric field reconstruction inside gas insulated transmission line by induced charge tomography," *IEEE Trans. Dielectr. Electr. Insul.*, vol. 27, no. 4, pp. 1372-1375, Aug. 2020, doi:10.1109/tdei.2020.008887.

[4] H. Okubo, M. Yoshida, T. Takahashi, T. Hoshino, M. Hikita and A. Miyazaki, "Partial discharge measurement in long distance SF_6 gas insulated transmission line (GIL)," *IEEE Trans. Power Deliv.*, vol. 18, no. 1, pp. 41-41, Jul. 1998, doi:10.1109/61.686960.

[5] Y. Zang *et al.*, "A novel optical localization method for partial discharge source using ANFIS virtual sensors and simulation fingerprint in GIL," *IEEE Trans. Instrum. Meas.*, no. 70, pp. 3522411, Jul. 2021, doi: 10.1109/tim.2021.3097856.

[6] W. Ding, K. Ochi, J. Suehiro, K. Imasaka, R. Hayashi and M. Hara,, "Factors affecting PD detection in GIS using a carbon nanotube gas sensor," *IEEE Trans. Dielectr. Electr. Insul.*, vol. 14, no. 3, pp. 718-725, Jun. 2007, doi:10.1109/tdei.2007.369536.

[7] X. Zhang, J. Tie, Q. Chen, P. Xiao and M. Zhou, "Pt-doped TiO2-based sensors for detecting SF_6 Decomposition Components," *IEEE Trans. Dielectr. Electr. Insul.*, vol. 22, no. 3, pp. 1559-1566, Jun. 2015, doi:10.1109/tdei.2015.7116351.

[8] F. Zeng, Z. Lei, X. Yang, J. Tang, Q. Yao and Y. Miao, "Evaluating DC partial discharge with SF_6 decomposition characteristics," *IEEE Trans. Power Deliv.*, vol. 34, no. 4, pp. 1383-1392, Feb. 2019, doi:10.1109/tpwrd.2019.2900508.

[9] J. Gao, Y. Zhang, X. Li, G. Shi and Y. Zhang, "Quantitative detection of multicomponent SF_6 decomposition products based on Fourier transform infrared spectroscopy combined with CARS-ELM algorithm," *IEEE Trans. Instrum. Meas.*, vol. 71, pp. 1-8, Jul. 2022, doi:10.1109/tim.2022.3194933.

[10] M. Li, C. Zhou, and W. Zhou, "A revised model for calculating HV cable sheath current under short-circuit fault condition and its application for fault location—Part 1: The revised model," *IEEE Trans. Power Deliv.*, vol. 34, no. 4, pp. 1674-1683, Aug. 2019, doi:10.1109/tpwrd.2019.2918159.

[11] Y. Hu, Z. Zeng, J. Liu, J. Wang and W. Zhang, "Design of a distributed UHF sensor array system for PD detection and location in substation,"

IEEE Trans. Instrum. Meas., vol. PP, no. 99, pp. 1844-1851, Jun. 2019, doi: 10.1109/tim.2018.2890748.
[12] M. Avzayesh, M. F. Abdel-Hafez, W. M. F. Al-Masri, M. AlShabi and A. H. El-Hag, "A hybrid estimation-based technique for partial discharge localization," *IEEE Trans. Instrum. Meas.*, vol. 69, no. 11, pp. 8744-8753, Nov. 2020, doi: 10.1109/tim.2020.2999165.
[13] C. We *et al*., "Detection of SF_6 decomposition components under partial discharge by photoacoustic spectrometry and its temperature characteristic," *IEEE Trans. Instrum. Meas.*, vol. 65, no. 6, pp. 1343-1351, Jun. 2016, doi: 10.1109/tim.2013.2276474.
[14] H. Cheng et al., "Simultaneous detection of C_2H_2 and CO based on cantilever-enhanced photoacoustic spectroscopy," *IEEE Trans. Instrum. Meas.*, vol. 70, pp. 1-10, May. 2021, doi:10.1109/tim.2021.3080377.
[15] Y. Martin *et al*., "Detection of SF_6 decomposition products generated by DC corona discharge using a carbon nanotube gas sensor," *IEEE Trans. Dielectr. Electr. Insul.*, vol. 19, no. 2, pp. 671-676, Apr. 2012, doi:10.1109/tdei.2012.6180262.
[16] R. Qiu, *et al*., "Methods for alleviation of impacts of axial diffusion on decomposition products monitoring in gas‐insulated transmission lines," *High Volt.*, vol. 7, no. 1, pp. 41-51, Jul. 2022, doi:10.1049/hve2.12130.
[17] Q. Chen, Q. Li, and H. Cong, "Numerical calculation and correlative factors analysis on temperature distribution of GIS bus bar based on coupled multi-physics methodology combined with multiple boundary conditions," *Trans. China Electrotech. Soc.*, vol. 31, no. 17, pp. 187-195, Sept 2016, doi:10.3969/j.issn.1000-6753.2016.17.021.
[18] X. W. Wu, N. Q. Shu, H. T. Li and L. Li, "Contact temperature prediction in three-phase gas-insulated bus bars with the finite-element method," *IEEE Trans. Magn.*, vol. 50, no. 2, pp. 277-280, Feb. 2014, doi:10.1109/tmag.2013.2282033.
[19] M. Liu, J. Zou, R. Qiu, Z. Li and W. Zhou, "The computation of diffusion characteristics of decomposition gases in SF_6 and SF_6/N_2 within gas insulated transmission lines," *Trans. China Electrotech. Soc.*, vol. 35, pp. 52-63, Jun. 2020, doi:10.19595/j.cnki.1000-6753.tces.190544.
[20] J. Ham, Y. Kim, J. Kim and S. Song, "Heat transfer in gas-insulated bus bars," in *ASME-Heat Transfer Summer Conf.*, Las Vegas, NV, USA, 2003, pp. 453-459.
[21] D. Minaguchi, M. Ginno, K. Itaka, H. Furukawa, K. Nnomiya, and T. Hayashi, "Heat transfer characteristics of gas-insulated transmission lines," *IEEE Trans. Power Deliv.*, vol. 1, no. 1, pp. 1-9, Jan. 1986, doi:10.1109/tpwrd.1986.4307881.
[22] R. Greenkorn, *Momentum, heat, and mass transfer fundamentals*, 1st ed. ed., Boca Raton, FL, USA: CRC Press, 1999, pp. 843-963.

Rui Qiu was born in Harbin, China in 1992. He received the B.Sc. and master degrees from the Harbin University of Science and Technology, Harbin, China in 2015 and 2018, respectively. His research interests include the prediction of gas's dielectric strength, the decomposition and diffusion processes in SF_6 and its substitutes.

He is currently pursuing the Ph.D. degree with the school of Electrical Engineering and Automation, Wuhan University, Wuhan, China.

Wenjun Zhou (Member, IEEE) was born in Hanchuan, Hubei Province, China, in 1959. He got the Ph.D. degree in 1990 from Wuhan University of Hydraulic and Electrical Engineering, Wuhan, China. His research focuses on high voltage insulation and testing technology.

Currently, he is a professor in Wuhan University, Wuhan, China.

Prof. Zhou is a senior member of IEEE and a member of the High Voltage Committee of the Chinese Society of Electrical Engineering (CSEE).

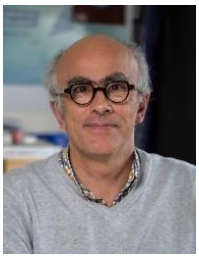

Pascal Brault was born in Le Blanc, France, in 1961. He got the Ph.D. degree in 1987 from University of Orleans, France. His major research interest focuses on molecular simulations for plasma processing, e.g. Plasma sputtering deposition, plasma polymers, and plasma treatment of wastewater.

Currently, he is a CNRS senior scientist in GREMI laboratory, CNRS–University of Orléans, France. He was awarded Alexander von Humboldt Fellow in 1992-1993.

Dr. Brault is a member of European Physical Society.

Yu Zheng (Member, IEEE) was born in Tianmen city, Hubei province, China, in 1992. He obtained Bachelor's degree in Electrical engineering and automation and Ph.D. degree in Electrical engineering from Wuhan University in 2014 and 2020. His research interests mainly are SF_6 alternative gases and digital twin for power equipment.

Currently, he is a postdoctoral fellow in Wuhan University.

Dr. Zheng is a member of IEEE and works as a secretary for IEEE PES T&D workshop of digital twin for power equipment.

GEN LI was born in China. He received the B.Sc. degree from Huazhong University of Science and Technology, Wuhan, China, in 2017, and the Master's degree from Wuhan Research Institute of Post and Telecommunication, Wuhan, China, in 2021. His research interests include fault location and condition monitoring of power cables.

He is currently working toward the Ph.D. degree from Wuhan University, Wuhan, China.

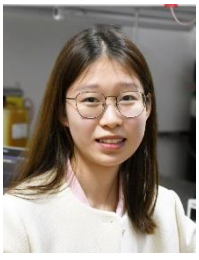

HAN Yang was born in Nantong, 331Jiangsu Province, China, in 2001.

Currently, she is studying at the School of Electrical Engineering and Automation of Wuhan University.

HAN LI was born in Wuhan, Hubei Province, China, in 1980. He received the B.Sc. degree from the Wuhan University, Wuhan, China, in 2002, the MSc degree from South China University of Technology, Guangzhou, China, in 2006 and PhD degree from Wuhan University, Wuhan, China in 2011. His research interest focuses on high voltage insulation and electrical testing technology, gas discharge and lightning physics.

Currently, he is an Associate Professor at the School of Electrical Engineering and Automation of Wuhan University.